Chapter 6
Modelling and MPC of the Proton Exchange Membrane Fuel Cell Using Wiener Models

Please cite the book:
Maciej Ławryńczuk: Nonlinear Predictive Control Using Wiener Models: Computationally Efficient Approaches for Polynomial and Neural Structures. Studies in Systems, Decision and Control, vol. 389, Springer, Cham, 2022.

Abstract This Chapter discusses simulation results of MPC algorithms based on Wiener models applied to the proton exchange membrane fuel cell. At first, the process is shortly described, identification of three structures of neural Wiener models and model selection are discussed. Efficiency of the polynomial Wiener model is also evaluated. Implementation details of different MPC algorithms are given. Next, efficiency of MPC algorithms is compared in terms of control quality and computational time.

6.1 Control of Proton Exchange Membrane Fuel Cells

Currently, the transport sector relies on combustion engines which use fossil fuels. Alas, it results in emission of greenhouse gases, which leads to serious environmental problems, i.e. air pollution, global warming, climate changes and destruction of the ozone layer. Zero-emission electric vehicles are available and their popularity grows. Typically, electric vehicles use batteries for energy storage. Unfortunately, such cars have a few disadvantages. Although they are zero-emission, the energy may be produced in a non-zero-emission process. Moreover, recharging of batteries takes long hours and the range is limited. An interesting alternative is to use a fuel cell for energy generation because, in such a case, the energy is produced in a really zero-emission environmentally friendly process and the tank is filled in minutes. Fuel cells are electrochemical devices that convert the chemical energy of a fuel (often hydrogen) and an oxidising agent (often oxygen) directly into electrical energy [16]. They have many significant advantages: high electrical efficiency, very low emission and quiet operation. Moreover, since fuel cells do not have moving parts, their life

cycle is very long. Fuel cells may be produced in different scales: from microwatts to megawatts, which makes them useful in numerous applications. Lastly, hydrogen necessary for fuel cells may be quite easily produced, so dependence on imported oil may be significantly reduced.

Among existing types of fuel cells [16], the Proton Exchange Membrane (PEM) fuel cells are preferred not only for mobile and vehicle applications, including cars, scooters, bicycles, boats and underwater vessels [1, 22] but also for stationary ones. This is because of low operation temperature (usually between 60-80 °C) which gives a fast start-up, simple and compact design as well as reliable operation. Since solid electrolyte is used, no electrolyte leakage is possible. The PEM fuel cells are considered to be very promising power sources and they are expected to become sound alternatives to conventional power generation methods.

It is necessary to point out that control of PEM fuel cells is a challenging task. Although there are examples of classical control methods applied to the PEM fuel cell, e.g. a linear state feedback controller [25] or a Sliding-Mode Controller (SMC) [15], the process is inherently nonlinear and linear controllers may give control accuracy below expectations. Hence, different nonlinear control strategies have been applied to the PEM fuel cell process: an adaptive Proportional-Integral-Derivative (PID) algorithm whose parameters are tuned on-line by a fuzzy logic system [2, 21] or by a neural network [7], an adaptive PID algorithm with a fuzzy logic feedforward compensator [5], a nonlinear state feedback controller [13], a fuzzy controller [19] and a look-up table [23]. Fractional complex-order controllers may be also used [29, 28]. Recently, MPC algorithms have been applied for the PEM fuel cell. In the literature, it is possible to find two categories of MPC:

1. The fully-fledged nonlinear MPC-NO algorithm [10, 26, 27, 35]. Such an approach may be very computationally demanding, its practical application may be impossible.
2. The classical LMPC algorithm based on a fixed (parameter-constant) linear model [3, 24]. In this approach, on-line calculations in MPC are not demanding (quadratic optimisation is used), but the resulting control quality may be not satisfactory because the process is nonlinear and the linear model used in MPC is only a very rough approximation of the nonlinear process.

The contribution of this Chapter is threefold:

1. Effectiveness of three Wiener structures is compared. It is necessary to point out that the Wiener model is a natural representation of the PEM process. A neural network of the MLP type is used in the static part of the Wiener models. In contrast to all Wiener model presented in Chapter 2 and discussed in other chapters of this book, in all described models of the PEM fuel cell, not only influence of the process input on the output is taken into account, but also the impact of the measured disturbance on the output is considered.
2. Effectiveness of the polynomial Wiener model is evaluated. The best structure chosen for the neural Wiener model is used; the only difference is utilisation of polynomials in place of neural networks in the nonlinear static part of the model.

3. Two nonlinear MPC algorithms for the PEM fuel cell are described: the MPC-NPSL and MPC-NPLT approaches. In contrast to the algorithms presented in [10, 26, 27, 35], in both algorithms computationally simple quadratic optimisation is used, full nonlinear optimisation is not necessary. The discussed algorithms are compared to the MPC-NO scheme in terms of control accuracy and computational time, inefficiency of the classical LMPC scheme is shown.

6.2 Description of the Proton Exchange Membrane Fuel Cell

In the general case, the model of the PEM fuel cell is quite complicated [25]. Hence, the tendency is to use simpler models for development of the control system [6, 4, 11, 30, 31, 33]. In this work, the PEM fuel cell model introduced in [33] and further discussed in [9, 14, 34] is considered. The PEM process has one manipulated variable (the input of the process) which is the input methane flow rate q (mol s^{-1}), one disturbance (the uncontrolled input) I which is the external current load (A) and one controlled variable (the output of the process) which is the stack output voltage V (V). The partial pressures of hydrogen, oxygen and water are denoted by p_{H_2}, p_{O_2} and p_{H_2O}, respectively (atm). The input hydrogen flow, the hydrogen reacted flow and the oxygen input flow are denoted by $q^{in}_{H_2}$, $q^{r}_{H_2}$ and $q^{in}_{O_2}$, respectively (mol s^{-1}).

The fundamental continuous-time model of the PEM system is defined by a set of transfer functions. The pressure of hydrogen is

$$p_{H_2} = \frac{1/K_{H_2}}{\tau_{H_2} s + 1} \left(q^{in}_{H_2} - 2K_r I \right) \tag{6.1}$$

where K_{H_2} and τ_{H_2} denote the valve molar constant for hydrogen and the response time of hydrogen flow, respectively. The input hydrogen flow obtained from the reformer is

$$q^{in}_{H_2} = \frac{CV}{(\tau_1 s + 1)(\tau_2 s + 1)} q \tag{6.2}$$

where q is the methane flow rate, CV, τ_1 and τ_2 are constants. Hence, from Eqs. (6.1) and (6.2), the pressure of hydrogen is

$$p_{H_2} = \frac{1/K_{H_2}}{\tau_{H_2} s + 1} \left(\frac{CV}{(\tau_1 s + 1)(\tau_2 s + 1)} q - 2K_r I \right) \tag{6.3}$$

The pressure of oxygen is

$$p_{O_2} = \frac{1/K_{O_2}}{\tau_{O_2} s + 1} \left(q_{O_2}^{in} - K_r I \right) \tag{6.4}$$

where K_{O_2} and τ_{O_2} denote the valve molar constant for oxygen and the response time of oxygen flow, respectively. The input flow rate of oxygen is

$$q_{O_2}^{in} = (1/\tau_{H\text{-}O}) q_{H_2}^{in} \tag{6.5}$$

where $\tau_{H\text{-}O}$ is the ration of hydrogen to oxygen. Using Eq. (6.2), the pressure of oxygen is

$$p_{O_2} = \frac{1/K_{O_2}}{\tau_{O_2} s + 1} \left(\frac{CV/\tau_{H\text{-}O}}{(\tau_1 s + 1)(\tau_2 s + 1)} q - K_r I \right) \tag{6.6}$$

The pressure of water is

$$p_{H_2O} = \frac{1/K_{H_2O}}{\tau_{H_2O} s + 1} q_{H_2}^{r} \tag{6.7}$$

where K_{H_2O} and τ_{H_2O} denote the valve molar constant for water and the response time of water flow, respectively. The hydrogen flow that reacts is

$$q_{H_2}^{r} = 2 K_r I \tag{6.8}$$

Hence, from Eqs. (6.7) and (6.8), the pressure of water is

$$p_{H_2O} = \frac{2K_r/K_{H_2O}}{\tau_{H_2O} s + 1} I \tag{6.9}$$

Finally, the stack output voltage is

$$V = E - \eta_{act} - \eta_{ohmic} \tag{6.10}$$

From the Nernst's equation

$$E = N_0 \left[E_0 + \frac{RT}{2F} \ln \frac{p_{H_2} \sqrt{p_{O_2}}}{p_{H_2O}} \right] \tag{6.11}$$

where N_0, E_0, R_0, T_0, F_0 denote the number of cells in series in the stack, the ideal standard potential, the universal gas constant, the absolute temperature and the Faraday's constant, respectively. The activation loses are defined by

$$\eta_{act} = B \log(CI) \tag{6.12}$$

where B and C are constants. The ohmic losses are

$$\eta_{ohmic} = R^{int} I \tag{6.13}$$

where R^{int} is the internal resistance.

Table 6.1 The fuel cell: the parameters of the fundamental continuous-time model

Parameter	Value	Unit	Description
B	0.04777	$1\ A^{-1}$	Activation voltage constant
C	0.0136	V	Activation voltage constant
CV	2	–	Conversion factor
E_0	0.6	V	No load voltage
F	96485	$C\ mol^{-1}$	Faraday's constant
K_{H_2}	4.22×10^{-3}	$mol\ s^{-1}\ atm^{-1}$	Hydrogen valve constant
K_{H_2O}	7.716×10^{-3}	$mol\ s^{-1}\ atm^{-1}$	Water time constant
$K_r = N_0/4F_0$	2.2802×10^{-3}	$mol\ s^{-1}\ A^{-1}$	Constant
K_{O_2}	2.11×10^{-2}	$mol\ s^{-1}\ atm^{-1}$	Oxygen time constant
N_0	88	–	Number of cells
R_0	8.314	$J\ mol^{-1}\ K^{-1}$	Universal gas constant
R^{int}	0.00303	Ω	Internal resistance
T_0	343	K	Absolute temperature
$\tau_1 = \tau_1$	2	s	Reformer time constants
τ_{H_2}	3.37	s	Hydrogen time constant
$\tau_{H\text{-}O}$	1.168	–	Hydrogen-oxygen flow ratio
τ_{H_2O}	18.418	s	Water time constant
τ_{O_2}	6.74	s	Oxygen time constant

Table 6.2 The fuel cell: the values of process variables for the initial operating point

Variable	Value	Unit
I	100	A
q	0.5	$mol\ s^{-1}$
p_{H_2}	5.9102	atm
p_{O_2}	39.4959	atm
p_{H_2O}	22.6160	atm
V	56.6179	V

The continuous-time fundamental model consists of Eqs. (6.2), (6.3), (6.6), (6.8), (6.9), (6.10), (6.11), (6.12) and (6.13). The values of parameters are given in Table 6.1. Table 6.2 gives the values of process variables for the initial operating point. Fig. 6.1 shows the structure of the continuous-time fundamental model of the process. The values of process input and disturbance signals are constrained

$$0.1\ mol\ s^{-1} \leq q \leq 2\ mol\ s^{-1} \tag{6.14}$$

$$50\ A \leq I \leq 150\ A \tag{6.15}$$

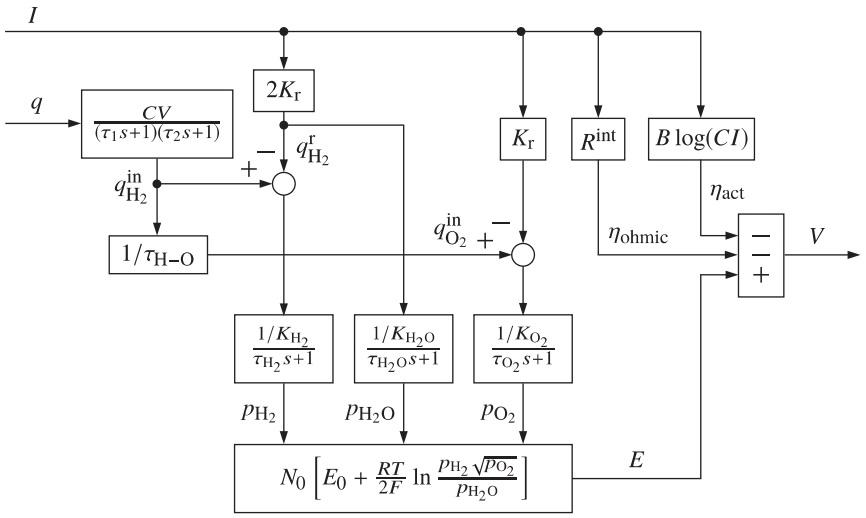

Fig. 6.1 The fuel cell: the structure of the continuous-time fundamental model

6.3 Modelling of the Proton Exchange Membrane Fuel Cell for MPC

It can be noted that the continuous-time fundamental model of the discussed PEM fuel cell is characterised by linear transfer functions (Eqs. (6.3), (6.6) and (6.9)), but the stack voltage is defined by the nonlinear steady-state Nernst's equation (6.11) and the activation losses are defined by the nonlinear equation (6.12). It means that the outputs of the linear dynamic part of the model are inputs of the nonlinear static one. Hence, it is straightforward to use the Wiener structure as an empirical model of the considered PEM fuel cell. We will evaluate performance of three structures of the neural Wiener model, for a different number of hidden nodes in the nonlinear static block and different order of dynamics of the linear model part. Furthermore, the chosen variant of the neural Wiener model will be compared with a corresponding polynomial Wiener structure.

For model identification, the manipulated variable of the process, q, the disturbance, I, and the output, V, are scaled

$$u = q - \bar{q},\ h = 0.01(I - \bar{I}),\ y = V - \overline{V} \tag{6.16}$$

where $\bar{q}$, $\bar{I}$ and $\overline{V}$ denote values of process variables for the initial operating point (Table 6.2). In the following part of this Chapter, three structures of the Wiener model for the PEM process are discussed.

Fig. 6.2 depicts the first structure of the neural Wiener model (the structure A). It consists of a linear dynamic block connected in series with a nonlinear static one. The linear block has two inputs (u – the controlled one, h – the uncontrolled one)

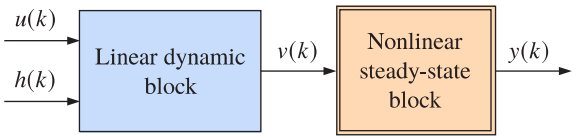

Fig. 6.2 The fuel cell: the structure A of the neural Wiener model

and one output, v, which is an auxiliary variable. The linear block is characterised by the equation

$$v(k) = \sum_{i=1}^{n_{\mathrm{B}}^1} b_i^1 u(k-i) + \sum_{i=0}^{n_{\mathrm{B}}^2} b_i^2 h(k-i) - \sum_{i=1}^{n_{\mathrm{A}}} a_i v(k-i) \tag{6.17}$$

The integers n_{A} and n_{B}^j, for $j = 1, 2$, define the order of the model dynamics. The constant parameters of the linear dynamic block are denoted by the real numbers a_i $(i = 1, \ldots, n_{\mathrm{A}})$, b_i^1 $(i = 1, \ldots, n_{\mathrm{B}}^1)$ and b_i^2 $(i = 0, \ldots, n_{\mathrm{B}}^1)$. It is important to note that the signal $v(k)$ depends directly on the signal $h(k)$ since the current, I, has an immediate impact on the voltage, V, (it is clear from Eqs. (6.10) and (6.12)). The output signal of the linear dynamic block is taken as the input of the static one. The nonlinear static part of the model is described by the general equation used in the case of the SISO process, i.e. Eq. (2.5). A neural network of the MLP type with one input, one hidden layer containing K units and one output is used as the differentiable function $g\colon \mathbb{R} \to \mathbb{R}$ [12]. The model output is

$$y(k) = w_0^2 + \sum_{l=1}^{K} w_l^2 \varphi\left(w_{l,0}^1 + w_{l,1}^1 v(k)\right) \tag{6.18}$$

where $\varphi\colon \mathbb{R} \to \mathbb{R}$ is a nonlinear transfer function (e.g. hyperbolic tangent). Weights of the network are denoted by $w_{l,m}^1$, $l = 1, \ldots, K$, $m = 0, 1$ and w_l^2, $l = 0, \ldots, K$, for the first and the second layers, respectively. The total number of weights is $3K + 1$.

Fig. 6.3 depicts the second structure of the neural Wiener model (the structure B). It consists of two linear dynamic blocks and a nonlinear static one, but unlike the structure A, the latter one has two inputs. The outputs of the linear blocks are characterised by the equations

$$v_1(k) = \sum_{i=1}^{n_{\mathrm{B}}^1} b_i^1 u(k-i) - \sum_{i=1}^{n_{\mathrm{A}}^1} a_i^1 v_1(k-i) \tag{6.19}$$

$$v_2(k) = \sum_{i=0}^{n_{\mathrm{B}}^2} b_i^2 h(k-i) - \sum_{i=1}^{n_{\mathrm{A}}^2} a_i^2 v_2(k-i) \tag{6.20}$$

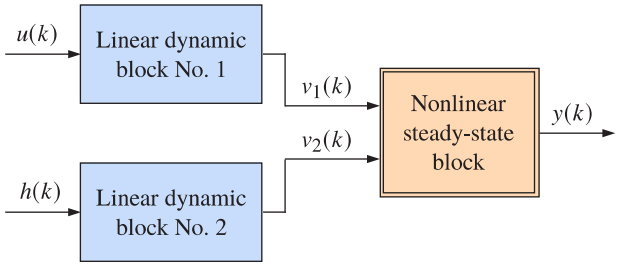

Fig. 6.3 The fuel cell: the structure B of the neural Wiener model

The integers n_{A}^j, n_{B}^j, $j = 1, 2$ define the order of the model dynamics. The constant parameters of the linear dynamic blocks are denoted by the real numbers a_i^1 ($i = 1, \ldots, n_{\mathrm{A}}^1$), a_i^2 ($i = 1, \ldots, n_{\mathrm{A}}^2$), b_i^1 ($i = 1, \ldots, n_{\mathrm{B}}^1$) and b_i^2 ($i = 0, \ldots, n_{\mathrm{B}}^1$). The signal $v_2(k)$ depends on the signal $h(k)$ since the current, I, has an immediate impact on the voltage, V. The nonlinear static block is described by the general equation

$$y(k) = g\left(v_1(k), v_2(k)\right) \tag{6.21}$$

A neural network of the MLP type with two inputs, one hidden layer containing K units and one output is used. The model output is

$$y(k) = w_0^2 + \sum_{l=1}^{K} w_l^2 \varphi\left(w_{l,0}^1 + w_{l,1}^1 v_1(k) + w_{l,2}^1 v_2(k)\right) \tag{6.22}$$

The weights of the network are denoted by $w_{l,j}^1$, $l = 1, \ldots, K$, $j = 0, 1, 2$ and w_l^2, $l = 0, \ldots, K$, for the first and the second layers, respectively. The overall number of weights is $4K + 1$.

Fig. 6.4 depicts the third structure of the neural Wiener model (the structure C). It has three linear dynamic blocks. They are characterised by the equations

$$v_1(k) = \sum_{i=1}^{n_{\mathrm{B}}^{11}} b_i^{11} u(k-i) + \sum_{i=1}^{n_{\mathrm{B}}^{12}} b_i^{12} h(k-i) - \sum_{i=1}^{n_{\mathrm{A}}^1} a_i^1 v_1(k-i) \tag{6.23}$$

$$v_2(k) = \sum_{i=1}^{n_{\mathrm{B}}^{21}} b_i^{21} u(k-i) + \sum_{i=1}^{n_{\mathrm{B}}^{22}} b_i^{22} h(k-i) - \sum_{i=1}^{n_{\mathrm{A}}^2} a_i^2 v_2(k-i) \tag{6.24}$$

$$v_3(k) = \sum_{i=1}^{n_{\mathrm{B}}^3} b_i^3 h(k-i) - \sum_{i=1}^{n_{\mathrm{A}}^3} a_i^3 v_3(k-i) \tag{6.25}$$

The integers n_{A}^j for $j = 1, 2, 3$, n_{B}^{ij} for $i = 1, 2$, $j = 1, 2$ and n_{B}^3 define the order of the model dynamics. The constant parameters of the linear dynamic blocks are denoted

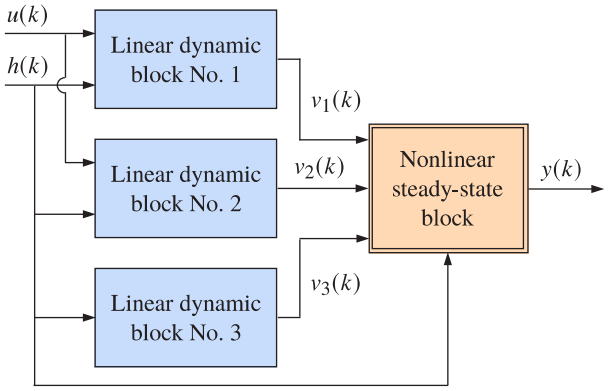

Fig. 6.4 The fuel cell: the structure C of the neural Wiener model

by the real numbers a_i^j $(i = 1, \ldots, n_{\mathrm{A}}^j,\ j = 1, 2, 3)$, b_i^{jl} $(i = 1, \ldots, n_{\mathrm{B}}^j,\ j = 1, 2,\ l = 1, 2)$ and b_i^3 $(i = 1, \ldots, n_{\mathrm{B}}^3)$. The nonlinear static block is described by the general equation

$$y(k) = g\left(v_1(k), v_2(k), v_3(k), h(k)\right) \tag{6.26}$$

Unlike two previously discussed model structures, in the structure C, the static block has an additional input which is the value of the disturbance signal, h, measured at the current sampling instant, k. A neural network of the MLP type with four inputs, one hidden layer containing K units and one output is used. The model output is

$$y(k) = w_0^2 + \sum_{l=1}^{K} w_l^2 \varphi\left(w_{l,0}^1 + \sum_{j=1}^{3} w_{l,j}^1 v_j(k) + w_{l,4}^1 h(k)\right) \tag{6.27}$$

Weights of the network are denoted by $w_{l,j}^1$, $l = 1, \ldots, K$, $j = 0, \ldots, 4$ and w_l^2, $l = 0, \ldots, K$, for the first and the second layers, respectively. The overall number of weights is $6K + 1$.

Next, we will discuss finding precise black-box models of the PEM fuel cell. A linear model and three discussed neural Wiener structures (A, B and C) are considered. All models are assessed in terms of the model error and the number of model parameters. During model identification, two data sets are used: the training data set and the validation one. The first of them is used only to find parameters of models, whereas the second one is used only to assess generalisation ability of models, i.e. how the model reacts when it is excited by a different data set than that used for identification. To obtain those two sets of data, the continuous-time fundamental model of the PEM process (defined by Eqs.(6.2), (6.3), (6.6), (6.8), (6.9), (6.10), (6.11), (6.12) and (6.13)) is simulated. The resulting system of differential equations is solved by the Runge-Kutta method of order 45. As the process input and disturbance signals, random sequences from the range characterised by Eqs.

(6.14) and (6.15)) are used. The process signals (i.e. the manipulated variable, q, the disturbance, I, and the controlled variable, V) are sampled with the sampling period equal to 1 second. The training and validation data sets are shown in Fig. 6.5, both sets consist of 3000 samples. Since identification of nonlinear Wiener models is a nonlinear optimisation problem, training is repeated as many as ten times for each model configuration and the results presented next are the best obtained.

All parameters of the Wiener model, i.e. the parameters of the dynamic part and weights of the neural network, are determined from an identification procedure. During identification, the classical model error is minimised. The model error is defined as the sum of squared differences between the model output and the data for all available data samples [8]. Since the model is nonlinear, optimisation of the model parameters is a nonlinear optimisation task which is solved off-line. For this purpose, the SQP algorithm is used [20], which makes it possible to take into account constraints during optimisation. To enforce stability of the Wiener model, the poles of the linear dynamic block are optimised subject to stability constraints (in the discrete-time domain, all poles must belong to the unit circle). Next, from the optimised poles, the model coefficients a_i^j are calculated. The values of b_i^j, $w_{l,m}^1$ and w_l^2 are directly calculated (optimised) with no constraints. Details of the optimisation procedure are described in [17].

At first, linear models of the process are considered. They have the following structure

$$y(k) = \sum_{i=1}^{n_{\mathrm{B}}^1} b_i^1 u(k-i) + \sum_{i=0}^{n_{\mathrm{B}}^2} b_i^2 h(k-i) - \sum_{i=1}^{n_{\mathrm{A}}} a_i y(k-i) \tag{6.28}$$

Table 6.3 compares linear models of different order of dynamics in terms of the number of parameters, the training error and the validation error. The first, the second, the third and the fourth order of dynamics is considered (it is defined as an integer number $n_{\mathrm{B}}^1 = n_{\mathrm{B}}^2 = n_{\mathrm{A}}$). As a compromise between model accuracy and complexity, the third-order model is chosen. The first part of Fig. 6.6 compares the validation data set vs. the output of the chosen linear model. The linear model is stable but not precise since there are significant differences between the model output and the data.

Table 6.3 The fuel cell: comparison of linear models of different order of dynamics in terms of the number of parameters (n_{par}), the training error (E_{train}) and the validation error (E_{val}); the chosen model is emphasised

Model order	n_{par}	E_{train}	E_{val}
1	4	1.4509×10^3	8.1537×10^2
2	7	1.4482×10^3	8.4352×10^2
3	10	1.0560×10^3	5.4921×10^2
4	13	9.5139×10^2	4.9939×10^2